Forcing of the Quarterdiurnal Tide

Ch. Geißler, Ch. Jacobi

Institute for Meteorology, Stephanstr. 3, 04103 Leipzig, E-Mail: christoph.geissler@uni-leipzig.de

Summary: Ensemble calculations for the period from 2000 to 2010 were carried out with the middle and upper atmosphere model (MUAM), and an analysis of the quarterdiurnal tide is performed. The global temporal and latitudinal distributions of the quarterdiurnal tide are modeled with MUAM, and their forcing mechanisms are examined. The quarterdiurnal tides show a similar distribution over the year in the northern and southern hemisphere, with maxima of the amplitude in late winter and spring as well as in autumn. In the latitude-height distribution is also shown that the largest amplitudes of the quarterdiurnal tide are seen at midlatitudes. Due to the decreasing density with height, there is a general increase of the tidal amplitudes with height. The results of the forcing analyses show that direct solar forcing is most important, but also that non-linear forcing and gravity wave interaction with other tides have a non-negligible influence on the quarterdiurnal tide in the middle and upper atmosphere.

Zusammenfassung: Mit dem Modell für die mittlere und obere Atmosphäre MUAM wurden Ensemble-Berechnungen für den Zeitraum 2000 bis 2010 durchgeführt und die vierteltägigen Gezeiten analysiert. Es wird auf die globale zeitliche und räumliche Verteilung der vierteltägigen Gezeiten eingegangen und deren Anregungsmechanismen untersucht. Die vierteltägigen Gezeiten zeigen einen ähnlichen Verlauf über das Jahr auf der Nord- und Südhalbkugel mit Maxima der Amplitude im späten Winter und Frühjahr sowie im Herbst. Ein ähnliches Bild zeigt sich auch für die Verteilung im Breiten-Höhen-Schnitt, wo die größten Amplituden der vierteltätigen Gezeiten in den mittleren Breiten zu finden sind. Aufgrund der abnehmenden Dichte mit der Höhe ist eine allgemeine Zunahme der Amplituden mit der Höhe zu beobachten. Es zeigte sich, dass der direkte solare Antrieb am stärksten ausgeprägt ist, aber auch, dass der nichtlinearer Antrieb und die Interaktion von Schwerewellen mit anderen Gezeiten einen nicht zu vernachlässigenden Einfluss auf die vierteltägigen Gezeiten in der mittleren und oberen Atmosphäre haben.

1. Introduction

Solar tides play an important role for the dynamics of the mesosphere and lower thermosphere (MLT) region. Tides have periods of a solar day and its subharmonics. They emerge mainly through absorption of solar radiation in the troposphere (water vapor) and stratosphere (ozone). The tidal amplitudes increase with height due to a decrease of density and conservation of energy (Chapman and Lindzen, 1970; Andrews et al., 1987). While diurnal, semidiurnal and terdiurnal tide are well understood, for the quarterdiurnal tide (QDT) there is still high research demand. There are some radar measurements available, e.g., at Collm (51°N, 13°E) and Obninsk (55°N, 37°E) as presented by Jacobi et al. (2017) and at Esrange (Smith et al., 2004), where analyses of the QDT had been made. Jacobi et

al. (2017) showed that the QDT at about 90 km has a maximum in zonal wind amplitude in January and during spring (April and May) of up to 3.5 ms^{-1} and in autumn (October and November) with about 3 ms^{-1}. Radar measurement at Esrange (68°N, 21°E) by Smith et al. (2004) show that the zonal wind amplitudes of the 6-hour tide between 85 km and 97 km are large in autumn, winter and early spring. Analyses of the QDT from satellite measurements (SABER) by Azeem et al. (2016) revealed that the QDT amplitudes in temperature increase with height and that there are maxima during the summer months (above 8 K) in the midlatitudes of the northern and southern hemisphere and near the equator. Liu et al. (2015) showed a ten years global distribution of the temperature amplitude of the 6h-tide in SABER measurements. They found that the largest amplitudes (up to 4 K) are seen in the midlatitudes of both hemispheres and at the equator. Liu et al. (2015) showed an increase of amplitude with height between 70 km and 110 km.

It is known from the terdiurnal tide that this tide can also be forced through interaction of other tidal components tide due to non-linear interaction, and due to possible interaction between tides and gravity waves (Beard et al., 1999); Akmaev, 2001; Du and Ward, 2010. Smith et al. (2004) showed in a model study that at 90 km the QDT has a maximum during autumn and winter months in the midlatitudes of the northern and southern hemisphere. They also showed that non-linear effects play an important role for the QDT. In a model run without solar forced 6h-tide they found the remaining non-linear forced tide makes up 50 % of the tide in the standard run (with solar forcing) during summer and one third in winter. Smith et al. (2004) did not look at the interaction between tides and gravity waves.

Generally, investigations of the 6-hr tide and its forcing mechanisms are rare. Therefore, it is necessary to conduct further model studies to see which respective influence solar forcing, gravity wave interaction, and nonlinear tide-tide interaction has on the QDT. It is also important to see if the results of Smith et al. (2004) can be confirmed by the MUAM model, and which forcings play a major role in the non-linear interaction. The remainder of this paper is structured as follows: The first part includes the model description and the used experimental setup. After that the results are presented and in the last part they are discussed.

2. Model Description and Experimental Setup

The middle and upper atmosphere model (MUAM) was used. MUAM is a 3D mechanistic global circulation primitive equation model of the middle atmosphere, which is based on the Cologne Model of the Middle Atmosphere-Leipzig Institute for Meteorology (COMMA-LIM, Fröhlich et al., 2003; Jacobi and Kürschner, 2006). In Pogoreltsev et al. (2007) the more recent version of the MUAM model is described. The model grid reaches from the surface (1000 hPa) up to the lower thermosphere (160 km in log-pressure height) with a vertical resolution of 2.842 km ($h = x \cdot H$ and $H = 7$ km as the scale height). Log-pressure heights are used with $x = ln\,(p_s/p)$ where p as pressure, $p_s = 1000$ hPa as a reference pressure. In the horizontal direction the model has a resolution of 5 × 5.625° and a time step of 225 s in the currently used 56-level version, which is following a Matsuno integration scheme (Matsuno, 1966). In the lower 30 km we nudge monthly mean ERA-Interim reanalyses of zonal mean temperature.

For the model experiments, ensemble runs are performed for 11 years (2000 to 2010). Stationary planetary waves at the lower boundary are not forced here to prevent coupling between stationary planetary waves and tides. The model includes gravity wave, solar, and infrared radiation parameterizations. Likewise, several ionospheric effects are parameterized. The model has a spin-up time of 120 model days. In that time zonal mean heating rates (no tides) form up a background climatology. The following 90 model days heating rates become zonally variable and tides begin to propagate. In the model there are three mechanisms that cause QDTs: solar heating, non-linear interaction between tides, and gravity wave-tidal interactions. Calculation of solar heating is following a Strobel parametrization (Strobel, 1978), which considers heating due to the most important gases like water vapor, carbon dioxide, ozone, oxygen and nitrogen. The carbon dioxide volume mixing ratio is taken from Mauna Loa Observatory data (NOAA ESRL Global Monitoring Division). The carbon dioxide mixing ratio, in the model assumed as horizontally invariable and constant up to 90 km is used in the model. The zonal mean ozone fields are taken from the Stratosphere-troposphere Processes And their Role in Climate project (SPARC; Randel and Wu, 2007) up to 50 km altitude. Non-linear effects can be evoked in the tendency equations of the model (e.g., Jakobs et al., 1986), i.e. in the temperature advection terms and in the zonal and meridional momentum equation terms. A gravity wave parametrization after Lindzen (1981) is used up to the mesosphere, for thermosphere and ionosphere a parametrization after Yigit et al. (2008) is used, which includes ionospheric effects like eddy diffusion. In our model experiment all three forcing processes are included. Carbon dioxide is fixed for the year 2005 (378 ppm for January), and this is also the case for the model ozone field. We performed 11 runs (ensemble) with different lower boundary conditions for the years 2000 to 2010 and calculated the 11-year mean and the standard deviation.

3. Model results

The results of the standard run that includes the solar, non-linear and the gravity wave forcing can be seen in Figure 1. QDT amplitudes of zonal wind (left), meridional wind (middle) and temperature (right) at 101 km altitude are shown for every latitude and month as mean over the 11-years of the ensemble run. Hatched areas show standard deviations larger than 0.1 ms^{-1} for zonal and meridional wind. Maxima of the QDT can be found in the southern and northern midlatitudes, and they reach values of 2 ms^{-1} for zonal and meridional wind amplitudes. Maxima can be seen during spring and autumn on both hemispheres, and also on the northern hemisphere in February and March, in May (only zonal wind), and in October and November. Maxima in the southern hemisphere occur in May, August and September. A second maximum in the zonal wind can be found in November around 50°S. This is the mostly the case at midlatitudes during autumn and winter months. The standard deviation is much stronger in the southern hemisphere because of a larger year-to-year variability. Maxima of the QDT amplitudes in temperature can be seen at midlatitudes in February, March and November in northern hemisphere and in May, August, and September in the southern hemisphere. Hatched areas show standard deviations larger than 0.05 K for temperature. Analogous to the zonal and meridional wind, the largest standard deviation can be seen in autumn and winter for the temperature amplitudes at midlatitudes.

To have a closer look at the tides two months are selected: September and November, to have a maximum at southern and northern hemisphere midlatitudes. The results as height–latitude plot are shown in Figure 2 for the amplitudes of zonal wind (left), meridional wind (middle) and temperature (right). Amplitudes for September (upper row) and November (lower row) are shown. The grey lines denote standard deviation in 0.2 ms^{-1} or 0.2 K, respectively. For September, the largest amplitudes occurs above 120 km at midlatitudes on both hemispheres, but the amplitudes in the southern hemisphere at midlatitudes are much stronger (above 5 ms^{-1}) for wind and temperature. The standard deviation over the northern hemisphere is slightly larger. Above 100 km, a third maximum occurs that can be found near the equator, but it is much smaller than the midlatitude ones.
The largest tides can be seen at midlatitudes. A maximum can be seen, mainly in meridional wind and temperature amplitudes, near the equator at higher altitudes. The same is visible for November, but the amplitude maxima are then seen at midlatitudes of the northern hemisphere. Overall, the amplitudes at midlatitudes of the northern hemisphere are stronger in November than in the midlatitudes of the southern hemisphere in September. Besides, the standard deviation is also considerably higher than in September and reaches up to 25% at midlatitudes of the northern hemisphere for the amplitudes in zonal wind. The different forcing terms of the QDT for September are shown in Fig. 3 and for November in Fig. 4, each scaled by density ($x = exp(-z/2 \cdot H)$). In the first row non-linear zonal wind advection and zonal gravity wave acceleration can be seen, in the second row non-linear meridional wind advection and meridional gravity wave acceleration is shown, in the third row non-linear temperature advection and gravity wave heating is presented, and the fourth row presents non-linear adiabatic heating and direct solar heating.
For September, important forcing terms of the QDT are the direct solar heating and the non-linear meridional wind advection. Forcing from solar heating takes place only below 80 km through water vapor and ozone absorption, and above 120 km due to extreme ultraviolet radiation absorption. The standard deviation (not shown) reaches up to 1×10^{-2} Kd^{-1} for the solar heating in the midlatitudes.

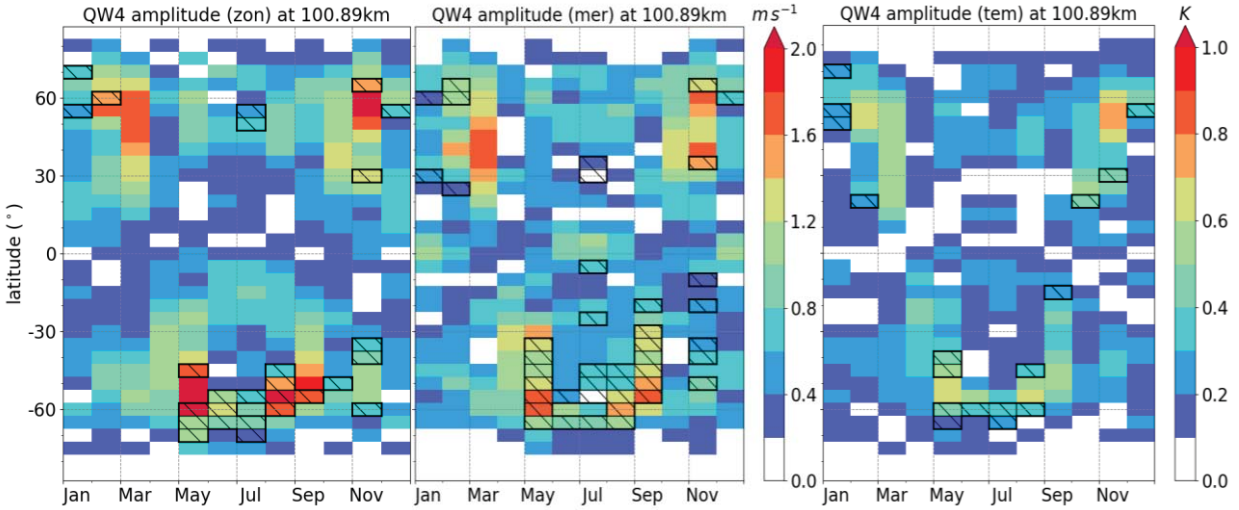

Fig. 1: 11 year mean quarterdiurnal tidal amplitudes of from MUAM simulations for zonal wind (left), meridional wind (mid) and temperature (right) for every month and latitude at 101 km. Hatched areas show months with standard deviation larger than 0.1 ms^{-1} for zonal and meridional wind and larger than 0.05 K for temperature.

Non-linear forcing occurs mainly at low latitudes, with a maximum between 10° and 20° on both hemispheres, up to the lower thermosphere. A secondary role compared with the other forcing terms plays the radiative cooling (not shown here), which can also effect a QDT. The standard deviation (not shown in the plot) is largest for the non-linear forcing of zonal and meridional wind advection in the middle and lower latitudes with up to 1×10^{-4} $ms^{-1}d^{-1}$ and up to 1×10^{-3} Kd^{-1} for temperature advection. Gravity wave forcing below 100 km arises from parameterized gravity waves, and shows largest values for zonal and meridional wind acceleration. Above 100 km the forcing is parameterized using by the Yigit type parametrization and shows maxima at midlatitudes for zonal wind acceleration and also in gravity wave heating above 100 km. The standard deviation of the zonal and meridional gravity wave acceleration has largest values up to 3×10^{-3} $ms^{-1}d^{-1}$ at midlatitudes below 100 km, and up to 3×10^{-2} Kd^{-1} for the gravity wave heating.

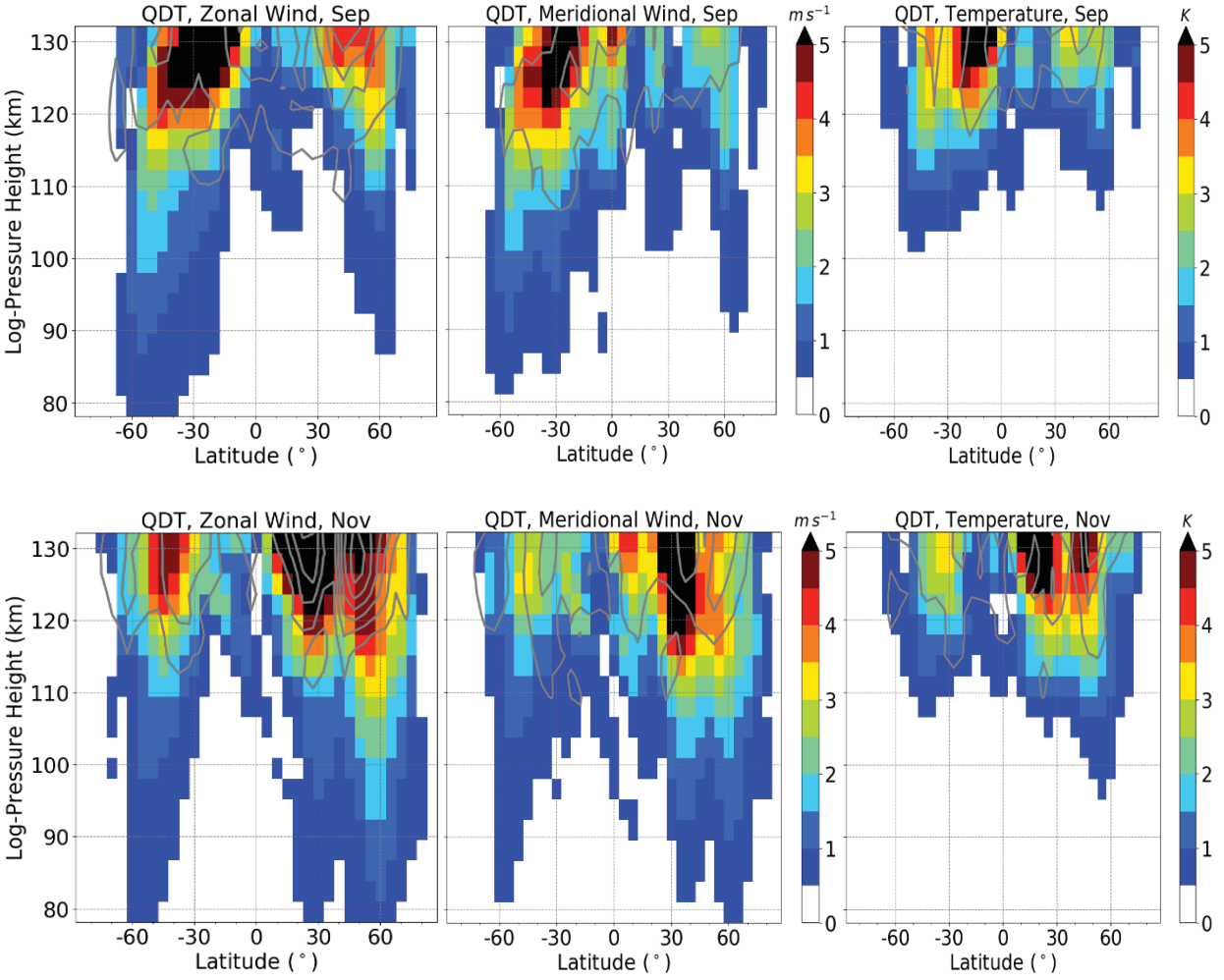

Fig. 2: 11 year mean quarterdiurnal tidal amplitudes of from MUAM simulations (colors) for zonal wind (left), meridional wind (middle) and temperature (right) at upper row for September and lower row for November.

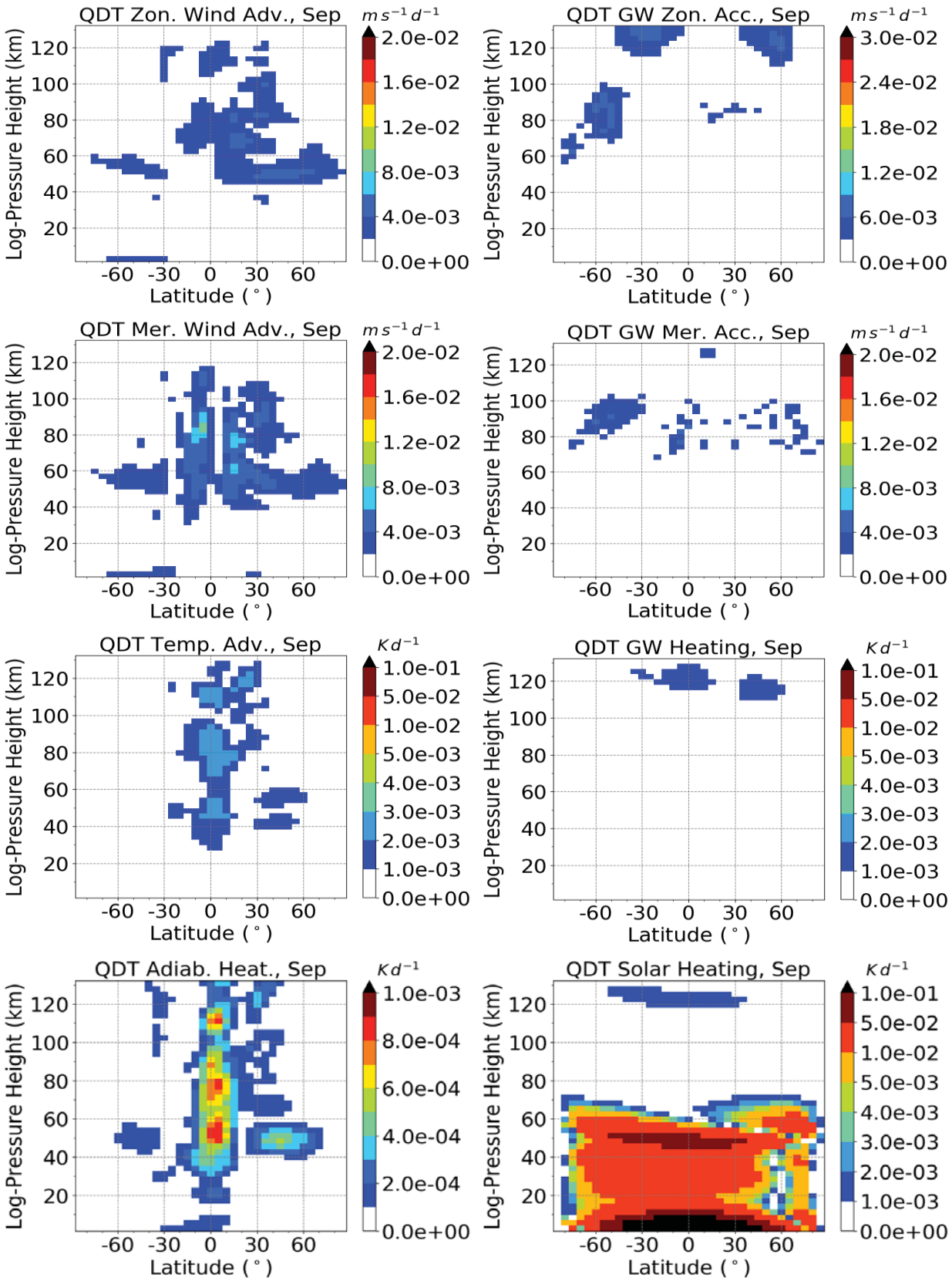

Fig. 3: Quarterdiurnal wavenumber 4 component of forcing terms scaled by density (from left to right) for September: 1st row: a) non-linear zonal wind advection, b) zonal GW acceleration, 2nd a) non-linear meridional wind advection, b) meridional GW acceleration. 3nd row: a) non-linear temperature advection, b) GW heating, 4th row a) non-linear adiabatic heating, b) direct solar heating.

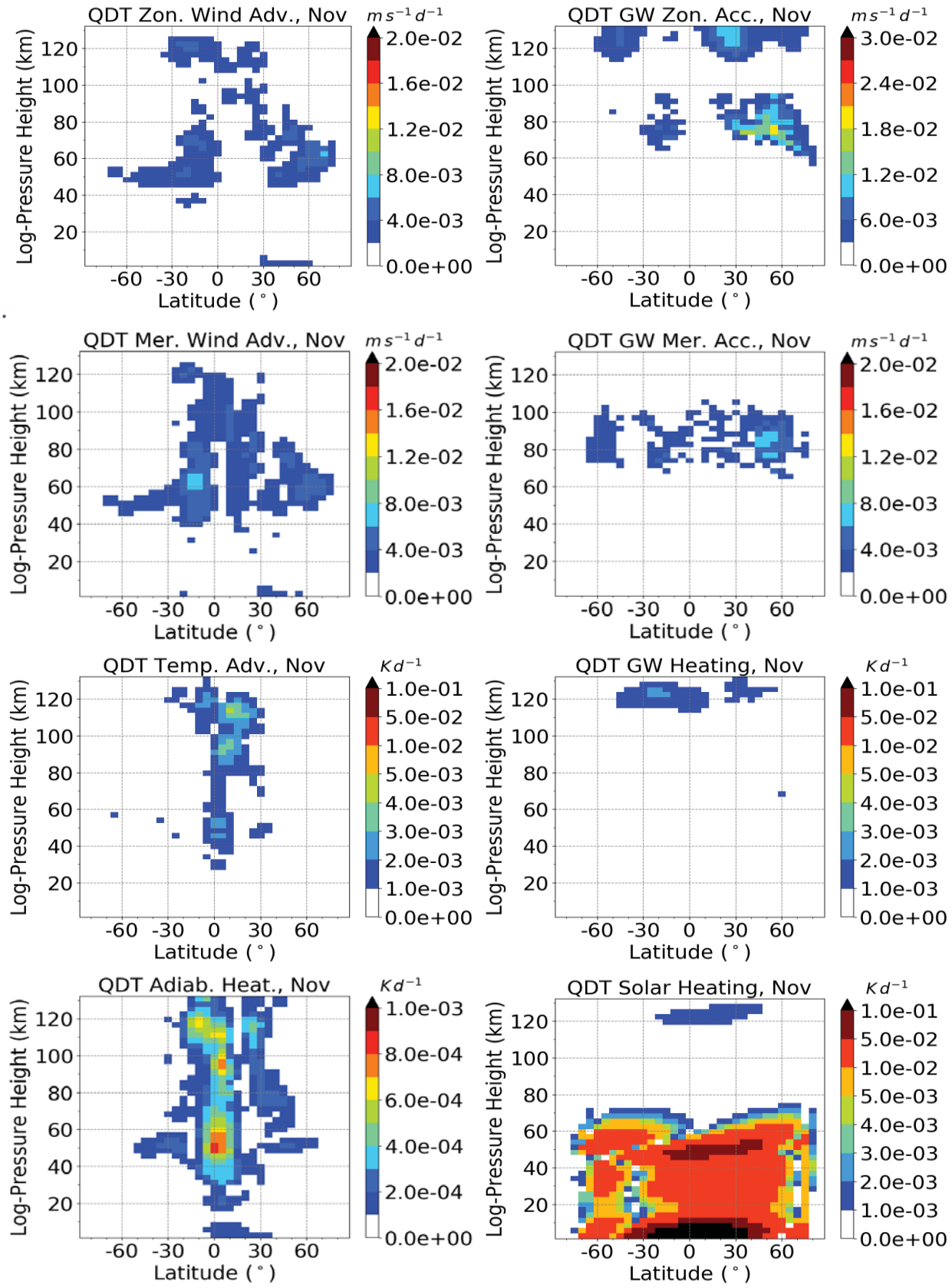

Fig. 4: Same as Fig. 3, but for November.

November (Fig. 4) shows a very similar spatial distribution of the forcing terms and their standard deviations compared to September. Solar heating is the most important forcing in November, but the influence of the gravity wave forcing is larger compared to September. Due to the stronger polar vortex in November the forcing of the gravity wave acceleration of zonal and meridional wind is much stronger in the northern midlatitudes than in September, but there is also a larger standard deviation because of larger year-to-year variability of the strength of polar vortex. The implication of this is that the amplitudes of the QDT must be stronger in November as in September and this can be seen in Fig. 2. In Fig. 3 showed also that the forcings at midlatitudes are larger in the northern hemisphere in November and in November with larger amplitudes in the southern midlatitudes. The weaker third maximum of the amplitudes, which can be seen near the equator in meridional wind and temperature amplitudes of the QDT, is caused from the forcing of non-linear effects like adiabatic heating and temperature advection.

5. Discussion and Conclusion

It could be seen from Figs. 3 and 4 that the direct solar forcing is the most important one for the QDT below 80 km, while non-linear forcing mainly occur at lower and middle latitudes between 20 km and 120 km. Gravity wave forcing plays a role above 80 km at midlatitudes. Smith et al. (2004) also shows that the solar forced QDT is largest. A less important role with much smaller resulting tide plays the non-linear forcing. Smith et al. (2004) indicate that the resulting tides are larger in the winter hemisphere as a consequence of a stronger non-linear forcing. Comparing the results from Fig. 1 with those of Smith et al. (2004) (ROSE model), Liu et al. (2015) (SABER/TIMED data), and Jacobi et al. (2017) (radar data), the amplitudes in the MUAM model are smaller. This could be caused by the lower meridional resolution of the MUAM model, so that the maxima of the QDT are not resolved correctly.

However, the distribution of maxima and minima of the QDT in Fig. 1 is similar than shown tides in other publications. In Smith et al. (2004) and Liu et al. (2015) the amplitudes have a maximum in the midlatitudes in spring and autumn (northern and southern hemisphere), which can also be seen in the MUAM model. The secondary maximum in May (northern hemisphere) and November (southern hemisphere) can be seen in Liu et al. (2015). In comparison with amplitudes from the meteor radar from Collm and Obninsk from Jacobi et al. (2017) for midlatitudes (Collm: 52°N, Obninsk: 55°N) it can be seen for zonal and meridional wind amplitudes that there are maxima in January, April, and November. But in the MUAM model is a time shift of two months in the maxima in late winter and spring. The temperature amplitudes for September and November in Fig. 2 show two larger maxima in the midlatitudes and a smaller one at the equator. This can also be seen in the ten years climatology from Liu et al. (2005), but the QDT amplitudes at 110 km show a stronger maximum at the equator than at northern midlatitude than in the MUAM model. A conclusion derived from the MUAM simulation and the discussion in comparison with other publications is that the direct solar forcing is the most important for the QDT. But monthly and seasonal variations in the strength of the non-linear and gravity wave forcing make these forcings only partially subordinate.

The largest QDT amplitudes can be seen at midlatitudes with maxima in late winter, spring (March and May), and autumn (November). The zonal mean of the amplitudes shows maxima in the midlatitudes and a second (smaller) one at the equator, but these maxima always increases with height up to 130 km. There are some differences in the amplitudes between the MUAM model and radar measurements for the maxima during winter and spring (time shift of one or two months). The height-latitude distribution from the MUAM model and the satellite data from Liu et al. (2015) show good comparison for the temperature amplitude of the QDT in the mesosphere and lower thermosphere.

Acknowledgements

ERA-Interim reanalyzes have been provided by ECMWF through www.ecmwf.int/en/research/climate-reanalysis/era-interim, and have been used in MUAM for assimilation in the troposphere as lower boundary condition. Carbon dioxide data were provided by NOAA: www.esrl.noaa.gov/gmd/ccgg/trends/. SPARC global ozone fields were provided by W.J. Randel (NCAR): ftp://sparc-ftp1.ceda.ac.uk/sparc/ref_clim/randel/o3data/.

References

Akmaev, R.,2001: Seasonal variations of the terdiurnal tide in the mesosphere and lower thermosphere: a modelstudy, Geophys. Res. Let., 28, 3817–3820, doi:10.1029/2001GL013002.

Andrews, D. G., Holton, J. R., and Leovy, C. B., 1987: Middle Atmosphere Dynamics, Academic Press Inc. (London) Ltd.

Azeem, I., Walterscheid. R. L., Crowley, G., Bishop, R. L., and Christensen, A. B., 2016: Observations of the migrating semidiurnal and quaddiurnal tides from the RAIDS/NIRS instrument, J. Geophys. Res. Space Physics, 121, doi:10.1002/2015JA022240.

Beard, A. G., Mitchell, N. J., Williams, P. J. S., and Kunitake, M., 1999: Non-linear interactions between tides and planetary waves resulting in periodic tidal variability, J. Atmos. Sol.-Terr. Phys., 61, 363–376, doi:10.1016/S1364-6826(99)00003-6.

Chapman, S., and Lindzen, R., 1970: Atmospheric tides - thermal and gravitational, p. 200, ix, D. Reidel Publishing Company (Dordrecht, Holland), 1970.

Du, J., and Ward, W., 2010: Terdiurnal tide in the extended Canadian Middle Atmospheric Model (CMAM), J. Geophys. Res., 115, D24, 106, doi:10.1029/2010JD014479.

Fröhlich, K., Pogoreltsev, A., and Jacobi, Ch., 2003: The 48 Layer COMMA-LIM Model: model description, new aspects, and climatology. Rep. Inst. Met. Leipzig 30, 157-185, http://meteo.physgeo.uni-leipzig.de/de/orga/LIM_VIII_HZ_Band_30.pdf.

Jacobi, Ch., and Kürschner, D., 2006: Long-term trends of MLT region winds over Central Europe, Physics and Chemistry of the Earth, Parts A/B/C, 31(1), 16-21, doi:10.1016/j.pce.2005.01.004.

Jacobi, Ch., Lilienthal, F., Geißler, Ch., and Krug, A., 2015: Long-term variability of mid-latitude mesosphere-lower thermosphere winds over Collm (51°N, 13°E), J. Atmos. Sol.-Terr. Phys., 136, 174-186, doi:10.1016/j.jastp.2015.05.006.

Jacobi, C., Krug, A., and Merzlyakov, E., 2017: Radar observations of the quarterdiurnal tide at midlatitudes: Seasonal and long-term variations, J. Atmos. Solar Terr. Phys., 163, 70-77, doi:10.1016/j.jastp.2017.05.014.

Jakobs, H. J., Bischof, M., Ebel, A., and Speth, P., 1986: Simulation of gravity wave effects under solstice conditions using a 3-D circulation model of the middle atmosphere, J. Atmos. Sol.-Terr. Phys., 48, 1203–1223, doi:10.1016/0021-9169(86)90040-1.

Lindzen, R. S., 1981: Turbulence and stress owing to gravity wave and tidal breakdown, J. Geophys. Res.: Oceans, 86, 9707–9714, doi:10.1029/JC086iC10p09707.

Liu, M. H., Xu, J. Y., Yue, J., and Jiang, G. Y., 2015: Global structure and seasonal variations of the migrating 6-h tide observed by SABER/TIMED, Science China: Earth Sciences, 58: 1216–1227, doi:10.1007/s11430-014-5046-6

Matsuno, T., 1966: Quasi-geostrophic motions in the equatorial area, J. Meteor. Soc. Japan, 44, 25-43, doi:10.2151/jmsj1965.44.1_25.

Pogoreltsev, A. I., Vlasov, A. A., Fröhlich, K., Jacobi, C., 2007: Planetary waves in Coupling the lower and upper atmosphere, J. Atmos. Sol.-Terr. Phys., 69, 2083-2101, doi:10.1016/j.jastp.2007.05.014.

Randel, W. J. and Wu, F.: A stratospheric ozone profile data set for 1979–2005, 2007: Variability, trends, and comparisons with column ozone data, J. Geophys. Res.: Atmos., 112, doi:10.1029/2006JD007339, d06313.

Smith, A. K., Pancheva, D. V., and Mitchell, N. J., 2004: Observations and modeling of the 6-hour tide in the upper mesosphere, J. Geophys. Res., 109, D10105, doi:10.1029/2003JD004421.

Strobel, D. F., 1978: Parameterization of the atmospheric heating rate from 15 to 120km due to O_2 and O_3 absorption of solar radiation, J. Geophys. Res.: Oceans, 83, 6225-6230, doi:10.1029/JC083iC12p06225.

Yigit, W., Aylward, A., and Medvedev, A., 2008: Parameterization of the effects of vertically propagating gravity waves for thermosphere general circulation models: Sensitivity study, J. Geophys. Res., 113, D19 106, doi:10.1029/2008JD010135.